

# Ideal Solar Cell Electrical Parameters and Ideality Factor Effect on the Efficiency

El Hadji Mamadou Keita\*, Fallou Mbaye, Abdoul Aziz Correa, Mamadou Dia, Cheikh Sene, Babacar Mbow

Laboratory of Semiconductors and Solar Energy, Physics Department, Faculty of Science and Technology, University Cheikh Anta Diop, Dakar, Senegal

## Email address:

elouazy@hotmail.fr (El Hadji Mamadou Keita)

\*Corresponding author

## To cite this article:

El Hadji Mamadou Keita, Fallou Mbaye, Abdoul Aziz Correa, Mamadou Dia, Cheikh Sene, Babacar Mbow. Ideal Solar Cell Electrical Parameters and Ideality Factor Effect on the Efficiency. *International Journal of Energy and Power Engineering*.

Vol. 12, No. 1, 2023, pp. 9-21. doi: 10.11648/j.ijepe.20231201.12

**Received:** December 9, 2022; **Accepted:** February 14, 2023; **Published:** March 28, 2023

---

**Abstract:** The determination of the electrical conversion efficiency ( $\eta_c$ ) is particularly important to evaluate the performance of a solar cell. For the evaluation of the efficiency by considering the ideal solar cell characterized by an absence of parasitic resistances and using the characteristic equation which corresponds to the equivalent electrical diagram, we determine the electrical parameters such as: the saturation current density ( $J_0$ ), the short-circuit current density ( $J_{sc}$ ), the open-circuit voltage ( $V_{oc}$ ), the maximum power density point ( $J_m$ ,  $V_m$ ) and the fill factor (FF). The saturation current density is determined using fundamental semiconductor notions. The effect of the ideality factor on the electrical efficiency and the various parameters is also highlighted. The results are applied to heterostructures based on  $CuInS_2$  and  $CuInSe_2$ . The performance of the cell increases with a raising of the ideality factor ( $\eta$ ) for the ideal solar cell model. By varying the ideality factor from 1 to 3, the calculated efficiency varies theoretically from 8.4% to 25.3% under AM1.5 solar spectrum for the structure based on  $CdS(n)/CuInS_2(p)$  named model (b) with a photocurrent density evaluated at  $17 \text{ mA.cm}^{-2}$  by numerical calculation method. The efficiency varies from 6.8% to 20.45% for the structure based on  $CdS(n)/CuInSe_2(p)$  named model (a) with a photocurrent density evaluated at  $31 \text{ mA.cm}^{-2}$  for the same used parameters. The open-circuit voltage varies from 0.5 V to 1.5 V for model (b) and from 0.27 V to 0.8 V for model (a). The results obtained (efficiency and electrical parameters) for each model remain within the range of experimental values published in the literature for solar cells based on chalcopyrite materials such as CIGS ( $CuIn_xGa_{1-x}Se_2$  or  $CuIn_xGa_{1-x}(S_ySe_{1-y})_2$ ), and thus allowing to validate the different methods established to model the studied phenomena.

**Keywords:** Ideal Solar Cell,  $CuInS_2 - CuInSe_2$ , Electrical Parameters, Ideality Factor, Efficiency

---

## 1. Introduction

The performance of a solar cell (in particular the electrical conversion efficiency) depends on the electrical parameters. The photodiode model is used usually to model the operation of a solar cell (in the case of inorganic materials). The models most used to model the operation of a photovoltaic cell are generally the single diode and double diode models [1-2]. The single diode model is the most used and given by the relation (1) and figure 1 [2-3]. This model takes into account the presence of the shunt  $R_{sh}$  and series  $R_s$

resistances, as well as the reducing of the diode quality due to the phenomenon of recombination of the electron-hole pairs, the quality of the diode is modeled by  $\eta$ . The current saturation current  $J_0$  results from transport phenomena and depends on the structure considered. The second model named double diode model is given by the relation (2) and figure 2 [3, 4]. The saturation current density  $J_{02}$  results from the recombination phenomena by trap centers in the space charge region.

$$J = J_{ph} - J_0 \left( e^{\frac{q(V+R_s J)}{\eta k T}} - 1 \right) - \frac{V + R_s J}{R_{sh}} \quad (1)$$

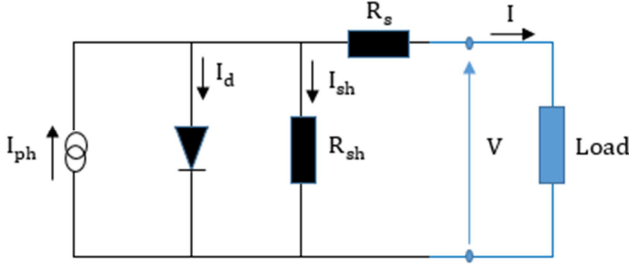


Figure 1. Equivalent electrical diagram of a single diode model.

$$J = J_{ph} - J_{01} \left( e^{\frac{q(V+R_s J)}{\eta_1 K T}} - 1 \right) - J_{02} \left( e^{\frac{q(V+R_s J)}{\eta_2 K T}} - 1 \right) - \frac{V+R_s J}{R_{sh}} \quad (2)$$

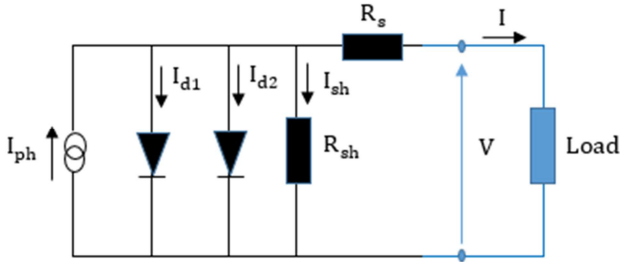


Figure 2. Equivalent electrical diagram of a double diode model.

The relation between the current supplied by the solar cell and the current density is:

$$I = J \times A_s \quad (3)$$

$A_s$  is the active surface of solar panels ( $m^2$ ),  $I$  is the current (A) delivered by the photovoltaic cell and  $J$  current density ( $A.m^{-2}$ ).

Generally the currents of the two diodes are combined to bring back to the single diode model [3]. The single diode model (as well as the double diode model) that describes the relation  $J$  and  $V$  by taken into account presence of parasitic resistances does not have an analytical solution, it is a transcendent equation. This model contains 5 physical parameters to be determined  $J_0$ ,  $R_{sh}$ ,  $R_s$ ,  $\eta$ ,  $J_{ph}$ , [5, 6, 7, 8] while the double diode model contains 7 parameters to be determined. Several models are used to solve this nonlinear equation [3, 9-13], these formulations are generally traditional or metaheuristic [10]. An analytical (traditional) method for solving this equation is proposed using the LambertW function [14-15]. Lambert's function  $W$  is a solution of the equation type:

$$we^w = x \quad (4)$$

The Lambert  $W$  function is defined as the multivalued function that satisfies:

$$w = \text{Lambert } W(x) \quad (5)$$

We have:

$$\text{Lambert } W(x)e^{\text{Lambert } W(x)} = x \quad (6)$$

The explicit (analytical) solution of the equation (1) can be expressed using the Lambert function  $W$ , it is given by [3, 5]:

$$J = -\frac{\eta V_{th}}{R_s} \text{Lambert } W[x] - \frac{V}{R_s} + \frac{R_s (J_0 + J_{ph}) + V}{R_s (1 + \frac{R_s}{R_{sh}})} \quad (7)$$

With:

$$V_{th} = \frac{KT}{q} \quad (8)$$

$$x = \frac{R_s J_0}{\eta V_{th} (1 + \frac{R_s}{R_{sh}})} e^{\left( \frac{R_s (J_0 + J_{ph}) + V}{\eta V_{th} (1 + \frac{R_s}{R_{sh}})} \right)} \quad (9)$$

Due to the implicit relation of the J-V equation, several other formulations (metaheuristic) to solve the equation of the single diode model have been developed to extract the parameters of the solar cell. We can mention among these methods the curve-fitting method, iterative 5-point method, analytical 5-point method [3, 16-22], PS optimization technique [3], Newton's method [23], genetic algorithm (GA) [10, 24], particle swarm optimization (PSO) [10, 25], simulated annealing (SA) [10, 26], etc.... However the results obtained with metaheuristic algorithms are better than those of traditional ones and each method has its limits [10, 27].

Several factors influence the current-voltage characteristic of a photovoltaic cell, such as the thickness of the active layers, the composition of the layers, the temperature of the cell, the illumination (flux of photons), etc... In chalcopyrite materials based on  $CuInSe_2/CuInS_2$ , alloys can be produced by substituting selenium (Se) atoms with sulfur (S) atoms forming the quaternary family  $CuIn(S_ySe_{1-y})_2$ , the band gap of these alloys varies between 1.04 eV and 1.53 eV. However, the rate of substitution of selenium atoms by sulfur atoms greatly influences the electrical parameters of the cell ( $R_{sh}$ ,  $R_s$ ,  $J_0$ ,  $\eta$  etc...). The efficiencies obtained with these alloys are generally less than 12% [28-29]. The electrical conductivity of  $CuInSe_2$  based solar cells also depends on the ratio Cu/In, this ratio influences the electrical parameters and the J-V characteristic [30-32]. The efficiency of ternary  $CuInSe_2/CuInS_2$  based solar cells are generally less than 15% [33-34]. Improvements of efficiency are obtained by substituting part of the Indium (In) atoms with Gallium (Ga) atoms leading to quaternary materials type  $CuIn_{1-x}Ga_xSe_2$  denoted CIGS whose forbidden energy band gap width varies between 1.04 and 1.68 eV by varying  $x$  from 0 to 1 [35-37]. Solar cells based on  $Cu(In,Ga)Se_2$  exhibit a record efficiency more than 20% [38]. They can be grown on Mo substrate (plate of Mo) or on a flexible plastic substrate [38-41]. The electrical parameters ( $R_{sh}$ ,  $R_s$ ,  $J_0$ ,  $\eta$  etc...) of a CIGS based solar cell and the J-V characteristic largely depend on  $x$ , the best efficiencies are obtained for  $x$  in order of 0.3 [42-46] resulting in band gaps between 1.1 and 1.2 eV. CIGS based solar cells are considered to be one of the most promising in the thin film sector because of its various characteristics (many features) such as their good efficiencies in terms of module and cell [47], simple manufacturing process (chemical bath, electrodeposition, ultrasonic spray pyrolysis, etc...) [42, 48], low manufacturing cost [42], excellent durability and stability [49]. CIGS based solar cells have other attractiveness such as flexibility and light weight [50-51], a high absorption coefficient in order of  $10^5 \text{ cm}^{-1}$

in the visible range [48-53] and direct band gap.

In this work we consider the model of the ideal solar cell. In this model the losses due to the presence of parasitic resistances in the materials which form the device, are not taken into account. The ideal case is represented by  $R_{sh}$  equal to infinity and  $R_s$  equal to zero in the single diode model. The model of the ideal solar cell presents an analytical resolution from equivalent model equation allowing to determine easily some of the characteristic parameters of the solar cell such as the short-circuit current density ( $J_{sc}$ ), the open-circuit voltage ( $V_{oc}$ ), the maximum power density point ( $J_m$ ,  $V_m$ ) and the fill factor (FF). The determination of the saturation current density ( $J_0$ ) is based on fundamental notions of semiconductor physics, the assumptions of quasi Fermi level and Shockley-Read are exploited for the determination of this parameter and we consider the regime of low injections of carriers [54-55].

## 2. Materials and Methods

### 2.1. Characteristic Equation of Ideal Solar Cell and Saturation Current Density

Without illumination, a photodiode operates like a conventional diode and obeys Schokley's relation [55]:

$$J_v = -J_0 \cdot (e^{qV_j/\eta KT} - 1) \quad (10)$$

$J_0$  is the saturation current density of the photodiode,  $K$  is the Boltzmann constant,  $\eta$  is the ideality factor,  $T$  is the temperature,  $q$  is the elementary charge. Under illumination, we take into account the photo-generated current density  $J_{ph}$  and obtain:

$$J = J_{ph} + J_v = J_{ph} - J_0 \cdot (e^{qV_j/\eta KT} - 1) \quad (11)$$

$J_{ph}$  is the photocurrent density generated by the illumination, its expression is given by previous studies [56-57]:

$$J_{ph} = \int_1^4 q \times F \times EQE \, dE \approx \frac{\delta E}{2} [J_{rp}(E_1) + J_{rp}(E_{m+1}) + 2 \sum_{i=2}^m J_{rp}(E_i)] \quad (12)$$

With:  $E \in [1, 4]$ ;  $E_1 = 1$ ;  $E_{m+1} = 4$ ;  $\delta E = \frac{E_{m+1} - E_1}{m}$   
 $E_{i+1} = E_i + i \cdot \delta E$  with:  $i: 1 \dots m$

$$J_0 = \frac{qD_n}{L_n} \frac{\left[ \text{ch}\left(\frac{H_p}{L_n}\right) \right]}{\text{sh}\left(\frac{H_p}{L_n}\right)} \cdot \frac{n_{ip}^2}{N_{ap}} + \frac{qD_p}{L_p} \frac{\left[ \text{ch}\left(\frac{H_n}{L_p}\right) \right]}{\text{sh}\left(\frac{H_n}{L_p}\right)} \cdot \frac{n_{in}^2}{N_{dn}} + \left( q \times \frac{1}{\tau_n} \frac{(N_{cn} \cdot N_{vn})^{\frac{1}{2}} \cdot e^{\frac{-E_{gn}}{2 \cdot K \cdot T}}}{2} \times w_n + q \times \frac{1}{\tau_p} \frac{(N_{cp} \cdot N_{vp})^{\frac{1}{2}} \cdot e^{\frac{-E_{gp}}{2 \cdot K \cdot T}}}{2} \times w_p \right) \quad (15)$$

With:

$$w_n \approx \left( \frac{2 N_{ap}}{q N_{dn}} \cdot \frac{\epsilon_n \cdot \epsilon_p}{\epsilon_n N_{dn} + \epsilon_p N_{ap}} \cdot V_d \right)^{\frac{1}{2}} \quad (16)$$

$$w_p \approx \left( \frac{2 N_{dn}}{q N_{ap}} \cdot \frac{\epsilon_n \cdot \epsilon_p}{\epsilon_n N_{dn} + \epsilon_p N_{ap}} \cdot V_d \right)^{\frac{1}{2}} \quad (17)$$

$$V_d = \frac{E_{gp} + E_{gn}}{2q} - \left[ \frac{E_{gn} - E_{gp}}{2q} + \chi_n - \chi_p + \frac{kT}{q} \ln \left( \frac{N_{cn} N_{vp}}{N_{dn} N_{ap}} \right) \right] \quad (18)$$

$$J_{rp} = q \times F \times EQE \quad (13)$$

$F$  represents the flux of photons versus the energy, it is expressed in  $\text{cm}^{-2} \cdot \text{s}^{-1} \cdot \text{eV}^{-1}$  [57].  $EQE$  is the external quantum efficiency.  $J$  is the current density supplied by the photodiode,  $V_j$  is the bias voltage across the n/p junction. The voltage  $V_j$  can be expressed as a function of the bias voltage  $V$  which appears at the terminals of the load supplied by the solar cell. For the model of the ideal solar cell, we have:  $V_j = V$ .

The characteristic equation of the ideal solar cell is given by:

$$J = J_{ph} - J_0 \cdot (e^{qV/\eta KT} - 1) \quad (14)$$

The corresponding equivalent electrical diagram is shown in figure 3 and the diagram of n/p junction is represented in figure 4.

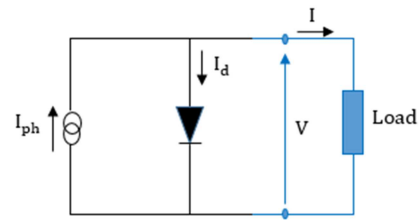


Figure 3. Equivalent electrical diagram of an ideal solar cell.

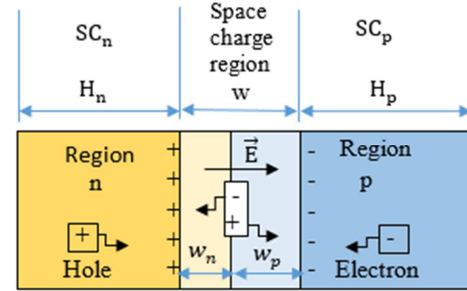


Figure 4. Junction n/p diagram.

Using fundamental notions of semiconductor physics, the assumptions of quasi Fermi level and Shockley-Read and the regime of low injections of carriers [54-55], the expression of saturation current density  $J_0$  for a n/p junction modeled by figure 4, can be written as:

The thickness of the space charge area is written as:

$$w = w_n + w_p \quad (19)$$

The intrinsic carrier densities in n and p regions are respectively given by:

$$n_{in} = (N_{cn} \cdot N_{vn})^{\frac{1}{2}} \cdot e^{\frac{-E_{gn}}{2 \cdot K \cdot T}} \quad (20)$$

$$n_{ip} = (N_{cp} \cdot N_{vp})^{\frac{1}{2}} \cdot e^{\frac{-E_{gp}}{2 \cdot K \cdot T}} \quad (21)$$

The various parameters used are defined in table 1.

**Table 1.** Nomenclature of the various parameters used.

$H_n, H_p$	$q \chi_n, q \chi_p$	$E_{gn}, E_{gp}$	$N_{cn}, N_{cp}$	$N_{vn}, N_{vp}$	$D_n, D_p$
thickness of the semiconductor n, p	electron affinity of the semiconductor n, p	energy band gap of the semiconductor n, p	density of states in the conduction band of the semiconductor n, p	density of states in the valence band of the semiconductor n, p	diffusion coefficient of electrons and holes
$N_{dn}$	$N_{ap}$	$n_{in}, n_{ip}$	$\tau_n, \tau_p$	$\epsilon_n, \epsilon_p$	$L_n, L_p$
concentration of the ionized donors in the semiconductor n	concentration of the ionized acceptors in the semiconductor p	concentration of intrinsic carriers in the semiconductor n, p	lifetime of the carriers in the space charge zone of the semiconductor n, p	electric permittivity of the semiconductor n, p	diffusion length of electrons and holes

**Table 2.** Data of used parameters.

Material	$N_v (cm^{-3})$	$N_c (cm^{-3})$	$E_g (eV)$	$\chi (eV)$	$\tau_n, \tau_p (s)$	$\epsilon (F \cdot m^{-1})$	$N_d, N_a (cm^{-3})$	$H_n, H_p (\mu m)$	$L_n, L_p (\mu m)$	$D_n, D_p (cm^2 \cdot s^{-1})$
CdS (n)	$5 \times 10^{19}$	$1 \times 10^{19}$	2.35	4.4	$10^{-8}$	$10 \times \epsilon_0$	$7.6 \times 10^{17}$	0.1	0.4	0.64
CuInS <sub>2</sub> (p)	$2 \times 10^{19}$	$5 \times 10^{18}$	1.57	4.04	$10^{-8}$	$15 \times \epsilon_0$	$1.9 \times 10^{17}$	1	3	5.13
CuInSe <sub>2</sub> (p)	$2 \times 10^{19}$	$5 \times 10^{18}$	1.04	4.58	$10^{-8}$	$15 \times \epsilon_0$	$1.9 \times 10^{17}$	1	3	10.27

$K = 1.38 \times 10^{-23} J \cdot K^{-1}$ ;  $\epsilon_0 = 8.85418782 \times 10^{-12} F \cdot m^{-1}$  ;  $q = 1.602 \times 10^{-19} C$  ;  $T = 300 K$ ;  $P_{solar} = 83.4 mW \cdot cm^{-2}$  (AM1.5) [58-59].

The values of table 2 are considered in the rest of this paper.

## 2.2. Ideal Solar Cell Model and Electrical Parameters

### 2.2.1. Quantum Efficiency and Photocurrent Current Density

Basing on previous studies [57], the expression of the external quantum efficiency  $EQE$  can be given by:

$$EQE = EQE_n + EQE_w + EQE_p \quad (22)$$

With:

$$EQE_n = \frac{\alpha_n(1-R)L_p}{(\alpha_n^2 L_p^2 - 1)} \times \left\{ \frac{\left( \frac{S_p L_p}{D_p} + \alpha_n L_p \right) - e^{-\alpha_n H_n} \left[ \frac{S_p L_p}{D_p} \text{ch} \left( \frac{H_n}{L_p} \right) + \text{sh} \left( \frac{H_n}{L_p} \right) \right]}{\frac{S_p L_p}{D_p} \text{sh} \left( \frac{H_n}{L_p} \right) + \text{ch} \left( \frac{H_n}{L_p} \right)} - \alpha_n L_p e^{-\alpha_n H_n} \right\} \quad (23)$$

$$EQE_w = -(1-R) \{ e^{-\alpha_n H_n} \times [e^{-\alpha_n w_n} - 1] + e^{-\alpha_n (H_n + w_n)} \times [e^{-\alpha_p w_p} - 1] \} \quad (24)$$

$$EQE_p = -\frac{\alpha_p L_n(1-R)}{(\alpha_p^2 L_n^2 - 1)} \times e^{[(\alpha_p - \alpha_n)(H_n + w_n)]} \left[ \frac{\left( \alpha_p L_n - \frac{S_n L_n}{D_n} \right) e^{-\alpha_p (H_n + H_p + w)}}{\frac{S_n L_n}{D_n} \text{sh} \left( \frac{H_p}{L_n} \right) + \text{ch} \left( \frac{H_p}{L_n} \right)} + \frac{e^{-\alpha_p (H_n + w)} \left[ \frac{S_n L_n}{D_n} \text{ch} \left( \frac{H_p}{L_n} \right) + \text{sh} \left( \frac{H_p}{L_n} \right) \right]}{\frac{S_n L_n}{D_n} \text{sh} \left( \frac{H_p}{L_n} \right) + \text{ch} \left( \frac{H_p}{L_n} \right)} - \alpha_p L_n e^{-\alpha_p (H_n + w)} \right] \quad (25)$$

$EQE_n$  represents the contribution of region n to the external quantum efficiency,  $EQE_p$  represents the contribution of region p to the external quantum efficiency, and  $EQE_w$  is the contribution of the space charge region to the external quantum efficiency.  $\alpha_n$  and  $\alpha_p$  represent respectively the absorption coefficients of the regions n and p, they depend on of the photon energy.  $S_n$  represents the recombination velocity of electrons at the surface of region p and  $S_p$  is the recombination velocity of holes at the surface of region n. R represents the reflection coefficient of the illuminated front layer.

The internal quantum efficiency IQE is given by:

$$IQE = IQE_n + IQE_w + IQE_p \quad (26)$$

With:

$$IQE_n = \frac{EQE_n}{1-R} \quad (27)$$

$$IQE_w = \frac{EQE_w}{1-R} \quad (28)$$

$$IQE_p = \frac{EQE_p}{1-R} \quad (29)$$

$IQE_n$  represents the contribution of region n to the internal quantum efficiency,  $IQE_p$  is the contribution of region p to the internal quantum efficiency and  $IQE_w$  represents the contribution of the space charge region to the internal quantum efficiency.

$$J_{ph} \approx q \times \frac{\delta E}{2} \times \{F(E_1) \times EQE(E_1) + F(E_{m+1}) \times EQE(E_{m+1}) + 2 \sum_{i=2}^m F(E_i) \times EQE(E_i)\} \quad (30)$$

We have taken for this calculation:

$$E_1 = 1 \text{ eV}; E_{m+1} = 3.88 \text{ eV}; \delta E = 0.03 \text{ eV}; m = 96$$

$$E_{i+1} = E_1 + i \cdot \delta E \text{ with } i: 1 \dots m$$

The discretized values of the external quantum efficiency of each model and of the solar spectrum AM1.5 noted F are represented in table 6.

### 2.2.2. Short-Circuit Current Density ( $J_{sc}$ )

The short-circuit current is the current obtained when the bias voltage V is zero, the equation (14) can be written as:

$$J_{sc} = J_{ph} \quad (31)$$

So the short-circuit current density corresponds to the photocurrent density generated by the solar cell.

### 2.2.3. Open Circuit Voltage ( $V_{oc}$ )

The open circuit voltage is the voltage that appears at the terminals of the solar cell when the current density J is zero. We obtain:

$$V_{oc} = \frac{\eta KT}{q} \ln \left( 1 + \frac{J_{ph}}{J_0} \right) \quad (32)$$

A decrease of the saturation current density  $J_0$  causes an increase of the open circuit voltage. We note in expression (32) that the open-circuit voltage increases with the ideality factor  $\eta$  and also with the photocurrent density  $J_{ph}$ . So it increases with lighting for a given temperature. Experience shows that an increase of the temperature results in a decrease of the open-circuit voltage [60].

### 2.2.4. Maximum Power Density Point (P)

The expression of the electrical power density P is given by:

$$P = V [J_{ph} - J_0 \cdot (e^{qV/\eta KT} - 1)] \quad (33)$$

The maximum power density point characterized by a current density  $J_m$  and a voltage  $V_m$  is defined by the relation:

$$\frac{dP}{dV} = 0 \quad (34)$$

We obtain:

$$V_{oc} = V_m + \frac{\eta KT}{q} \cdot \ln \left( 1 + \frac{q V_m}{\eta KT} \right) \quad (35)$$

Equation (35) is implicit, it can be solved by using a numerical method of resolution to determine  $V_m$ , we used the secant method [61]. The current density  $J_m$  is calculated from the following relation:

$$J_m = J_{ph} - J_0 \cdot (e^{q V_m / \eta KT} - 1) \quad (36)$$

The maximum power density  $P_m$  is given by:

The expression of the photocurrent density  $J_{ph}$  is given by the relation (12). For this calculation, we propose a numerical integration method and use the Newton quadrature. The photocurrent can be written as:

$$P_m = J_m \cdot V_m = (J_{ph} - J_0 \cdot (e^{q V_m / \eta KT} - 1)) \cdot V_m \quad (37)$$

The optimal load  $R_{optimal}$  is defined by:

$$R_{optimal} = \frac{V_m}{J_m} = \frac{V_m}{J_{ph} - J_0 \cdot (e^{q V_m / \eta KT} - 1)} \quad (38)$$

### 2.2.5. Fill Factor (FF)

The fill factor is given by the relation:

$$FF = \frac{P_m}{J_{sc} \cdot V_{oc}} \quad (39)$$

It can be written as:

$$FF = \frac{(J_{ph} - J_0 \cdot (e^{q V_m / \eta KT} - 1)) \cdot V_m}{J_{ph} \cdot (V_m + \frac{\eta KT}{q} \ln(1 + \frac{q V_m}{\eta KT}))} \quad (40)$$

### 2.2.6. Electrical Conversion Efficiency ( $\eta_c$ )

The electrical conversion efficiency of the photovoltaic cells is given by:

$$\eta_c = \frac{P_m}{P_{solar}} = \frac{FF \times V_{oc} \times J_{sc}}{P_{solar}} \quad (41)$$

$P_{solar}$  is the solar radiation ( $W/m^2$ ),  $P_{solar} = 100 \text{ mW} \cdot \text{cm}^{-2}$  under standard conditions (AM 1.5 G) and  $P_{solar} = 83,4 \text{ mW} \cdot \text{cm}^{-2}$  under AM 1.5 solar spectrum [58-59].

In the case of an ideal solar cell, the electrical conversion efficiency can be written as:

$$\eta_c = \frac{P_m}{P_{solar}} = \frac{(J_{ph} - J_0 \cdot (e^{q V_m / \eta KT} - 1)) \cdot V_m}{P_{solar}} \quad (42)$$

So we can write:

$$\eta_c = \frac{FF J_{ph} \cdot (V_m + \frac{\eta KT}{q} \ln(1 + \frac{q V_m}{\eta KT}))}{P_{solar}} \quad (43)$$

## 3. Results and Discussion

The results obtained are applied to the heterojunctions CdS(n)/CuInSe<sub>2</sub>(p) named model (a) and CdS(n)/CuInS<sub>2</sub>(p) named model (b). We apply the established results to plot the internal and external quantum efficiencies, the current density - voltage characteristic noted J (V) (J is the current density supplied by the solar cell and V the voltage at its terminals) and determine theoretically the characteristic of electrical parameters of solar cells.

From the data in table 2 and the equations (15-18), we determine the saturation current density  $J_0$ , it is estimated at  $J_0 = 4.117 \times 10^{-8} \text{ mA} \cdot \text{cm}^{-2}$  for a junction CdS(n)/CuInS<sub>2</sub>

(p) and at  $J_0 = 1.169 \times 10^{-3} \text{ mA} \cdot \text{cm}^{-2}$  for a junction CdS(n)/CuInSe<sub>2</sub>(p). According to the same considered parameters and using equation (18), the diffusion voltage  $V_d$  for the two structures is approximately equal to 1.033 V. The intrinsic carrier densities (equations 20 and 21) in CdS layer is estimated at  $4.011 \times 10^{-1} \text{ cm}^{-3}$ , in CuInS<sub>2</sub> layer at  $6.424 \cdot 10^5 \text{ cm}^{-3}$ , in CuInSe<sub>2</sub> layer at  $1.825 \times 10^{10} \text{ cm}^{-3}$ .

The photocurrent density  $J_{ph}$  is calculated using equation (22-25 and 30) and tables 2 and 6, it is estimated at  $17 \text{ mA} \cdot \text{cm}^{-2}$  for the junction CdS(n)/CuInS<sub>2</sub>(p), and it is estimated at  $31 \text{ mA} \cdot \text{cm}^{-2}$  for the junction CdS(n)/CuInSe<sub>2</sub>(p) under spectrum AM1.5.

### 3.1. Spectral Response Curves

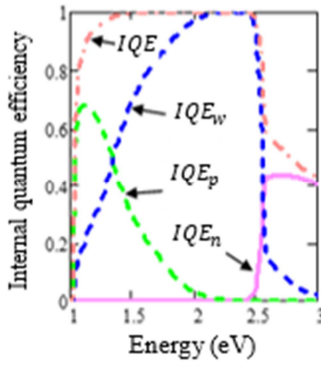


**Figure 5.** Internal quantum efficiency vs. photon energy: contribution of the different regions of the solar cell (region n, region p and space charge region). Model (a) CdS(n)/CuInSe<sub>2</sub>(p).

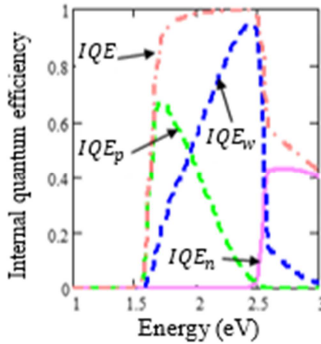


**Figure 6.** Internal quantum efficiency vs. photon energy: contribution of the different regions of the solar cell (region n, region p and space charge region). Model (b) CdS(n)/CuInS<sub>2</sub>(p).

Figures 5 and 6 represent the contribution of each region to the internal quantum efficiency versus the photon energy. In figure 7 we compare the external quantum efficiency of each model using a window layer based on ZnO, the influence of ZnO layer on the external quantum efficiency is neglected only its reflection coefficient has been taken into account. The solar cells are sensitive to the spectrum ranging from near infrared to visible. The band gaps of CuInS<sub>2</sub> and CuInSe<sub>2</sub> are respectively in order of 1.57 eV and 1.04 eV. We note that the response of the cells depend widely on the space charge region (IQE<sub>w</sub>) and the region p (IQE<sub>p</sub>). The discretized values of the energy, the photon flux and the external quantum efficiency in figure 7 allow to determine photocurrent density  $J_{ph}$  by using a numerical integration method (equation 30). Table 6

indicates the discretized values and is represented in appendix.

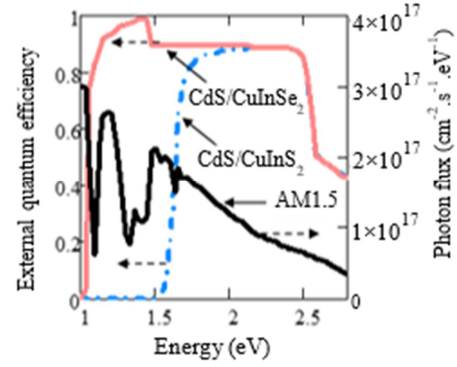


**Figure 7.** AM1.5 photon flux and external quantum efficiency vs. photon energy: comparison between model (a) CdS(n)/CuInSe<sub>2</sub>(p) and model (b) CdS(n)/CuInS<sub>2</sub>(p).

### 3.2. Current - Voltage Characteristic

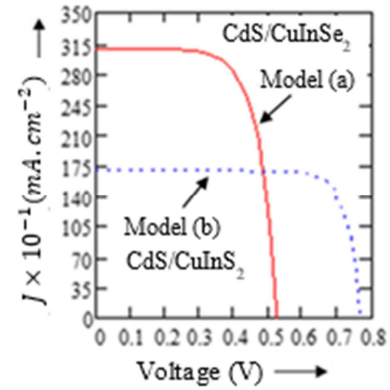


**Figure 8.** Comparative study of the evolution of the current density  $J$  versus bias voltage  $V$  for the two models.

Case of Ideal solar cell ( $R_s = 0 \Omega \cdot \text{cm}^2$  and  $R_{SH} = \infty \Omega \cdot \text{cm}^2$ )

Model (a): CdS(n)/CuInSe<sub>2</sub>(p) ( $J_0 = 1.169 \times 10^{-3} \text{ mA} \cdot \text{cm}^{-2}$ ;  $J_{ph} = 31 \text{ mA} \cdot \text{cm}^{-2}$ ;  $\eta = 2$ )

Model (b): CdS(n)/CuInS<sub>2</sub>(p) ( $J_0 = 4.117 \times 10^{-8} \text{ mA} \cdot \text{cm}^{-2}$ ;  $J_{ph} = 17 \text{ mA} \cdot \text{cm}^{-2}$ ;  $\eta = 1.5$ )

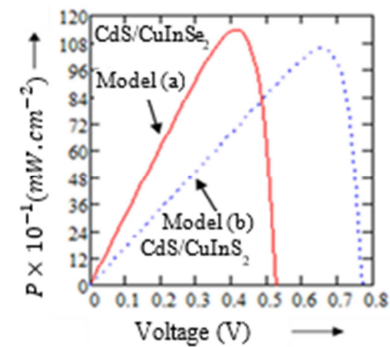


**Figure 9.** Comparative study of the evolution of the electrical power density  $P$  versus bias voltage  $V$  for the two models.

Case of Ideal solar cell ( $R_s = 0 \Omega \cdot \text{cm}^2$  and  $R_{SH} = \infty \Omega \cdot \text{cm}^2$ )

Model (a): CdS(n)/CuInSe<sub>2</sub>(p) ( $J_0 = 1.169 \times 10^{-3} \text{ mA} \cdot \text{cm}^{-2}$ ;  $J_{ph} = 31 \text{ mA} \cdot \text{cm}^{-2}$ ;  $\eta = 2$ )

Model (b): CdS(n)/CuInS<sub>2</sub>(p) ( $J_0 = 4.117 \times 10^{-8} \text{ mA} \cdot \text{cm}^{-2}$ ;  $J_{ph} = 17 \text{ mA} \cdot \text{cm}^{-2}$ ;  $\eta = 1.5$ )



In figure 8, we compare by considering the ideal case, the profiles of the current densities  $J$  versus the bias voltage  $V$  for the two models (a) and (b). In figure 9 we compare the profiles of the electrical powers  $P$  versus the bias voltage  $V$ . Regarding the ideality factor ( $\eta$ ) for these graphs, we have considered some values taken from the literature [62-64]. The characteristic electrical parameters of each model, resulting from this comparative study are summarized in table 3. We note that the calculated values of the electrical parameters for the two models are in the same magnitude order of those published in the literature [65].

### 3.3. Ideality Factor Effect on the Performance of the Ideal Solar Cell

In Figures 10-13, we study the effect of the ideality factor on the performance of the ideal solar cell. In figures 10 and 11, we respectively represent the evolution of the current density and the electrical power density versus the bias voltage for different values of the ideality factor  $\eta$  (varying from 1 to 3) for the model (b) CdS(n)/CuInS<sub>2</sub>(p) considering the ideal case ( $R_S = 0 \Omega \cdot \text{cm}^2$  and  $R_{SH} = \infty \Omega \cdot \text{cm}^2$ ). In Figures 12 and 13 the same studies are done for the model (a) CdS(n)/CuInSe<sub>2</sub>(p).

We note that the performance of the ideal solar cell increases with a raising of the ideality factor of the photodiode. Indeed, this improvement is explained by the fact that an increase of the ideality factor  $\eta$  reduces the diode current caused by the forward bias voltage. Thus, this allows an increase of the open-circuit voltage  $V_{oc}$ . So the maximum electrical power density of the solar cell increases with the ideality factor  $\eta$ . It should be noted that unlike the photovoltaic operating mode (solar cell in generator mode), the performance of the diode in dark conditions (absence of illumination) and under forward bias voltage (receiver mode) is reduced by an raising of the ideality factor  $\eta$ .

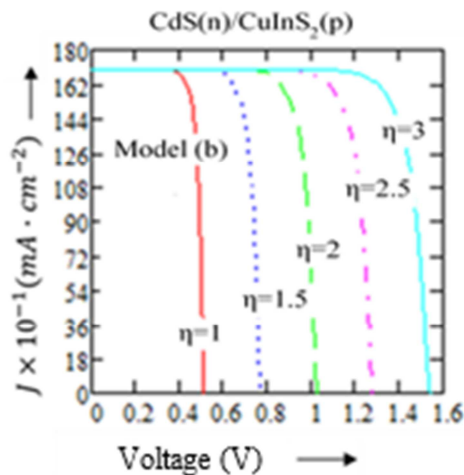


**Figure 10.** Evolution of the current density  $J$  versus bias voltage  $V$  for different values of the ideality factor ( $\eta = 1$  to 3).

( $J_0 = 4.117 \times 10^{-8} \text{ mA} \cdot \text{cm}^{-2}$ ;  $J_{ph} = 17 \text{ mA} \cdot \text{cm}^{-2}$  ;  $R_{SH} = \infty \Omega \cdot \text{cm}^2$ ;  $R_S = 0 \Omega \cdot \text{cm}^2$ )  
Model (b): CdS(n)/CuInS<sub>2</sub>(p)

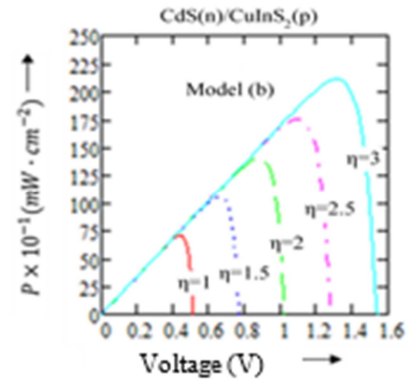


**Figure 11.** Evolution of the electrical power density  $P$  versus bias voltage  $V$  for different values of the ideality factor ( $\eta = 1$  to 3).

( $J_0 = 4.117 \times 10^{-8} \text{ mA} \cdot \text{cm}^{-2}$ ;  $J_{ph} = 17 \text{ mA} \cdot \text{cm}^{-2}$  ;  $R_{SH} = \infty \Omega \cdot \text{cm}^2$ ;  $R_S = 0 \Omega \cdot \text{cm}^2$ )  
Model (b): CdS(n)/CuInS<sub>2</sub>(p)

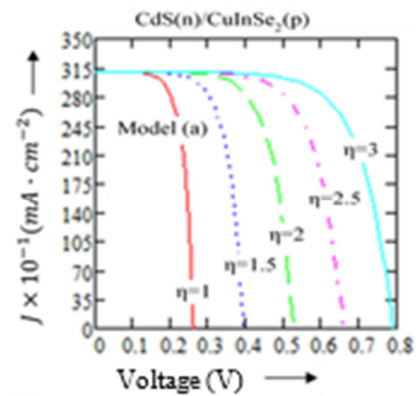


**Figure 12.** Evolution of the current density  $J$  versus bias voltage  $V$  for different values of the ideality factor ( $\eta = 1$  to 3)

( $J_0 = 1.169 \times 10^{-3} \text{ mA} \cdot \text{cm}^{-2}$ ;  $J_{ph} = 31 \text{ mA} \cdot \text{cm}^{-2}$  ;  $R_{SH} = \infty \Omega \cdot \text{cm}^2$ ;  $R_S = 0 \Omega \cdot \text{cm}^2$ )  
Model (a): CdS(n)/CuInSe<sub>2</sub>(p)

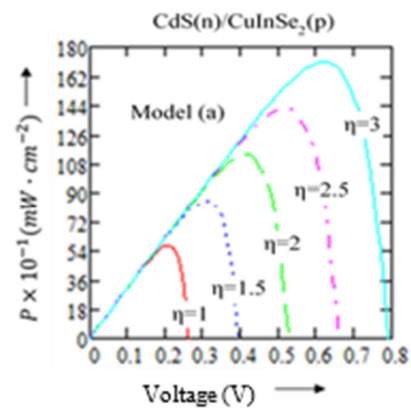


**Figure 13.** Evolution of the electrical power density  $P$  versus bias voltage  $V$  for different values of the ideality factor ( $\eta = 1$  to 3).

( $J_0 = 1.169 \times 10^{-3} \text{ mA} \cdot \text{cm}^{-2}$ ;  $J_{ph} = 31 \text{ mA} \cdot \text{cm}^{-2}$  ;  $R_{SH} = \infty \Omega \cdot \text{cm}^2$ ;  $R_S = 0 \Omega \cdot \text{cm}^2$ )  
Model (a): CdS(n)/CuInSe<sub>2</sub>(p)

**Table 3.** Electrical parameters of models (a) and (b) considering the ideal solar cell model (taken from figures 8 and 9).

Model	$R_S$ ( $\Omega.cm^2$ )	$R_{SH}$ ( $\Omega.cm^2$ )	$\eta$	$J_m$ ( $m A.cm^{-2}$ )	$V_m$ (V)	$P_m$ ( $mW.cm^{-2}$ )	$R_{optimal}$ ( $\Omega.cm^2$ )	$J_{sc}$ ( $m A.cm^{-2}$ )	$V_{oc}$ (V)	$FF$	$\eta_c$ (%)
CdS/CuInS <sub>2</sub>	0	$\infty$	1.5	16.053	0.657	10.547	40.927	17	0.769	0.807	12.646
CdS/CuInSe <sub>2</sub>	0	$\infty$	2	27.5526	0.413	11.379	14.989	31	0.526	0.698	13.644

**Table 4.** Characteristic electrical parameters of mode (b) for different values of the ideality factor  $\eta$  considering the ideal solar cell model (taken from figures 10 and 11).

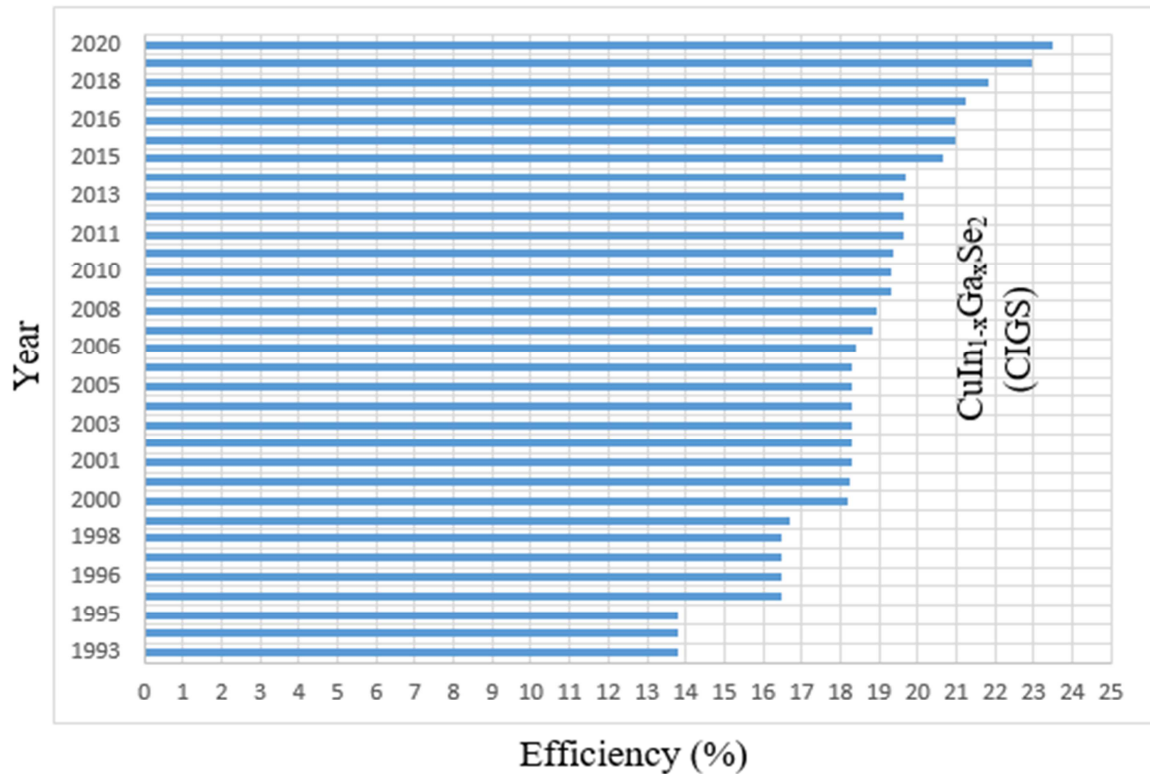
Structure	$R_S$ ( $\Omega.cm^2$ )	$R_{SH}$ ( $\Omega.cm^2$ )	$\eta$	$J_m$ ( $m A.cm^{-2}$ )	$V_m$ (V)	$P_m$ ( $mW.cm^{-2}$ )	$R_{optimal}$ ( $\Omega.cm^2$ )	$J_{sc}$ ( $m A.cm^{-2}$ )	$V_{oc}$ (V)	$FF$	$\eta_c$ (%)
CdS/CuInS <sub>2</sub>	0	$\infty$	1	16.053	0.438	7.031	27.285	17	0.513	0.8062	8.431
CdS/CuInS <sub>2</sub>	0	$\infty$	1.5	16.053	0.657	10.547	40.927	17	0.769	0.8068	12.646
CdS/CuInS <sub>2</sub>	0	$\infty$	2	16.053	0.876	14.062	54.569	17	1.025	0.807	16.861
CdS/CuInS <sub>2</sub>	0	$\infty$	2.5	16.053	1.095	17.578	68.211	17	1.282	0.8065	21.077
CdS/CuInS <sub>2</sub>	0	$\infty$	3	16.053	1.314	21.094	81.854	17	1.538	0.8068	25.292

**Table 5.** Characteristic electrical parameters of model (a) for different values of the ideality factor  $\eta$  considering the ideal solar cell model (taken from figures 12 and 13).

Structure	$R_S$ ( $\Omega.cm^2$ )	$R_{SH}$ ( $\Omega.cm^2$ )	$\eta$	$J_m$ ( $m A.cm^{-2}$ )	$V_m$ (V)	$P_m$ ( $mW.cm^{-2}$ )	$R_{optimal}$ ( $\Omega.cm^2$ )	$J_{sc}$ ( $m A.cm^{-2}$ )	$V_{oc}$ (V)	$FF$	$\eta_c$ (%)
CdS/CuInSe <sub>2</sub>	0	$\infty$	1	27.5526	0.206	5.676	7.477	31	0.263	0.6962	6.8
CdS/CuInSe <sub>2</sub>	0	$\infty$	1.5	27.5526	0.31	8.541	11.251	31	0.395	0.6975	10.241
CdS/CuInSe <sub>2</sub>	0	$\infty$	2	27.5526	0.413	11.379	14.989	31	0.526	0.6978	13.644
CdS/CuInSe <sub>2</sub>	0	$\infty$	2.5	27.5526	0.516	14.217	18.728	31	0.658	0.6969	17.047
CdS/CuInSe <sub>2</sub>	0	$\infty$	3	27.5526	0.619	17.055	22.466	31	0.79	0.6964	20.45

The various characteristic electrical parameters of the solar cells resulting from figures 10 and 11 are summarized in table 4 for the model (b) CdS(n)/CuInS<sub>2</sub>(p) and the electrical

parameters resulting from figures 12 and 13 are summarized in table 5 for the model (a) CdS(n)/CuInSe<sub>2</sub>(p).

**Figure 14.** Bar histogram graph of the efficiency of solar cells based on  $Cu(In,Ga)(Se,S)_2$  during some years (1993-2021) adapted from [66].



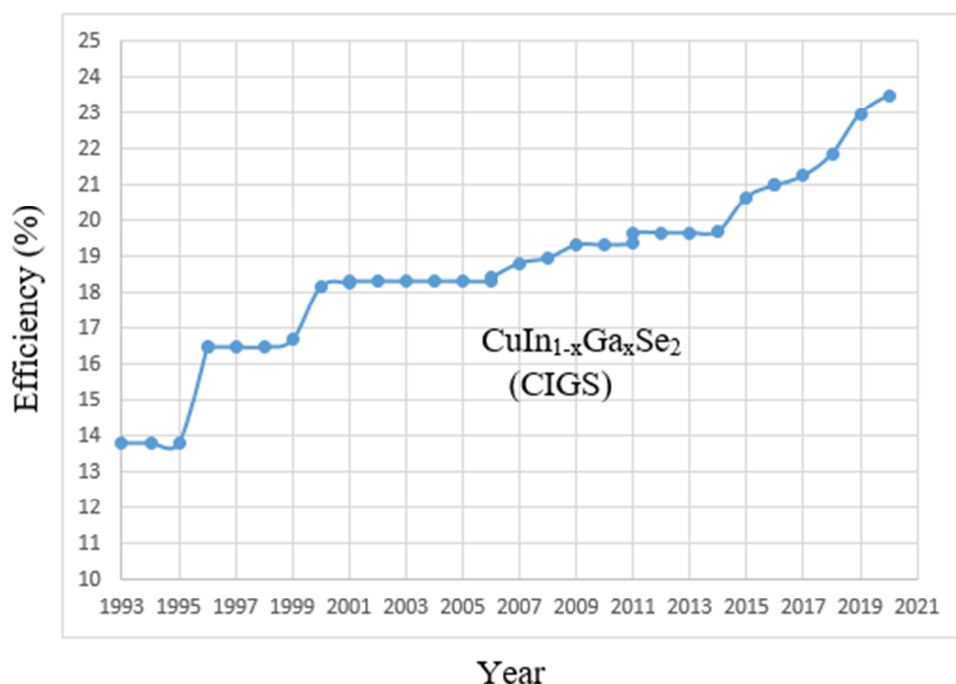


**Figure 15.** Evolution of the efficiency of solar cells based on  $\text{Cu(In,Ga)(Se,S)}_2$  during some years (1993 to 2021) adapted from [66].

In figures 14 and 15 we represent the evolution of the efficiency of solar cells based on  $\text{Cu(In,Ga)(Se,S)}_2$  (CIGS) during some years (1993-2021). A notable advance in conversion efficiency is observed, the efficiencies of these photovoltaic cells now exceed 22% for CIGS based solar cells with the introduction of gallium atom (Ga) and remain lower than 15% (without its introduction) for solar cells based on  $\text{CuInSe}_2/\text{CuInS}_2$ . However, our results obtained (table 3 to table 5) are well within magnitude order of solar cells based on chalcopyrite materials  $\text{CuIn}_x\text{Ga}_{1-x}(\text{S}_y\text{Se}_{1-y})_2$ .

The variations of the parameters in the modeling study reflect several factors which influence the efficiency of the solar cells such as the transition from one alloy to another (variation of  $x$  and  $y$ ), the influence of doping elements, the introduction of passivation elements (incorporation of sodium Na, aluminum oxide  $\text{Al}_2\text{O}_3$ , chemical treatments etc...), the influence of the defects (which can be passivated by the introduction of certain elements), the treatment of the layers by annealing etc.... However, the theoretical limit efficiencies of solar cells for single junctions are predicted by the theory of Shockley and Queisser, which determines the limit of the conversion around 33.7% corresponding to an optimal gap of the order of 1.34 eV for an incident solar power of  $1000 \text{ W.m}^{-2}$  (AM 1.5 G solar spectrum) [59].

## 4. Conclusion

The determination of electrical parameters (saturation current density, photocurrent density, short-circuit current density, open-circuit voltage, fill factor, maximum power density point) of an ideal photovoltaic cell (absence of parasitic resistances) has been essentially developed in this paper. The determination of these parameters is important to determine the energy conversion efficiency relative to solar

irradiation AM1.5 and to evaluate the performance of the solar cell. The results obtained were applied to heterostructures based on  $\text{CuInS}_2$  and  $\text{CuInSe}_2$ :  $\text{CdS(n)/CuInSe}_2(\text{p})$  named model (a) and  $\text{CdS(n)/CuInS}_2(\text{p})$  named model (b). The influence of the ideality factor on the current - voltage characteristic is also highlighted. The raising of this parameter increases the open circuit voltage and improves the performance of the ideal solar cell.

With the model (b)  $\text{CdS(n)/CuInS}_2(\text{p})$ , in the ideal case (no parasitic resistances) and depending on the used parameters, we obtain under AM 1.5 solar spectrum, a theoretical conversion efficiency ranging from 8.4% to 25.3% for ideality factors ranging between 1 and 3. The photocurrent density used with this model is evaluated at  $17 \text{ mA.cm}^{-2}$  based on the considered parameters, it corresponds to the short-circuit current density. The open-circuit voltage varies from 0.5 V to 1.5 V.

For the model (a)  $\text{CdS(n)/CuInSe}_2(\text{p})$ , we obtain in ideal case, a theoretical conversion efficiency varying from 6.8% to 20.45% for ideality factors ranging from 1 to 3 under the same solar irradiation conditions according to the used parameters. The photocurrent density is estimated at  $31 \text{ mA.cm}^{-2}$  based on the considered parameters, it corresponds to the short-circuit current density. The open-circuit voltage varies from 0.27 V to 0.8 V.

However, the results obtained for each model (photocurrent density, short-circuit current density, open-circuit voltage, fill factor, maximum power point, saturation current density) are in agreement and remain within the range of experimental values published in the literature for ideality factor lower than 2 and predict results for ideality factor greater than 2. Globally, the results obtained remain within the range of experimental values published in the literature for solar cells based on CIGS ( $\text{CuIn}_x\text{Ga}_{1-x}\text{Se}_2$  or  $\text{CuIn}_x\text{Ga}_{1-x}(\text{S}_y\text{Se}_{1-y})_2$ ) allowing to validate

the different methods established to model the studied phenomena.

## Appendix

**Table 6.** Discretized values of the energy ( $E$ ), the external quantum efficiency ( $EQE$ ) and the photon flux ( $F$ ).

$E$ (eV)	$EQE$ CdS/CuInS <sub>2</sub>	$EQE$ CdS/CuInSe <sub>2</sub>	$F \times 10^{17}$ (cm <sup>-2</sup> .s <sup>-1</sup> .eV <sup>-1</sup> )	$E$ (eV)	$EQE$ CdS/CuInS <sub>2</sub>	$EQE$ CdS/CuInSe <sub>2</sub>	$F \times 10^{17}$ (cm <sup>-2</sup> .s <sup>-1</sup> .eV <sup>-1</sup> )
1	0	0	3.006	2.47	0.877	0.877	0.677
1.03	0	0.033	3.004	2.5	0.854	0.854	0.644
1.06	0	0.749	1.884	2.53	0.795	0.795	0.624
1.09	0	0.834	0.632	2.56	0.653	0.653	0.608
1.12	0	0.879	2.221	2.59	0.507	0.507	0.575
1.15	0	0.911	2.58	2.62	0.496	0.496	0.544
1.18	0	0.927	2.632	2.65	0.484	0.484	0.518
1.21	0	0.94	2.631	2.68	0.473	0.473	0.493
1.24	0	0.951	2.139	2.71	0.462	0.462	0.462
1.27	0	0.961	1.625	2.74	0.451	0.451	0.418
1.3	0	0.969	0.889	2.77	0.44	0.44	0.377
1.33	0	0.976	0.763	2.8	0.43	0.43	0.338
1.36	0	0.981	1.248	2.83	0.419	0.419	0.304
1.39	0	0.985	1.132	2.86	0.409	0.409	0.293
1.42	0	0.987	1.071	2.89	0.399	0.399	0.282
1.45	0	0.99	1.144	2.92	0.389	0.389	0.271
1.48	0	0.892	2.1	2.95	0.379	0.379	0.261
1.51	0.004	0.893	2.117	2.98	0.37	0.37	0.23
1.54	0.013	0.893	1.96	3.01	0.361	0.361	0.184
1.57	0.04	0.894	2.031	3.04	0.352	0.352	0.142
1.6	0.197	0.894	1.943	3.07	0.344	0.344	0.134
1.63	0.422	0.894	1.499	3.1	0.335	0.335	0.126
1.66	0.642	0.894	1.841	3.13	0.327	0.327	0.119
1.69	0.742	0.894	1.708	3.16	0.318	0.318	0.112
1.72	0.8	0.894	1.721	3.19	0.311	0.311	0.106
1.75	0.827	0.894	1.66	3.22	0.303	0.303	0.1
1.78	0.846	0.894	1.604	3.25	0.296	0.296	0.094
1.81	0.854	0.894	1.55	3.28	0.29	0.29	0.088
1.84	0.86	0.894	1.498	3.31	0.283	0.283	0.083
1.87	0.865	0.894	1.435	3.34	0.278	0.278	0.077
1.9	0.869	0.893	1.374	3.37	0.273	0.273	0.072
1.93	0.872	0.893	1.317	3.4	0.271	0.271	0.068
1.96	0.875	0.893	1.263	3.43	0.269	0.269	0.063
1.99	0.877	0.892	1.213	3.46	0.267	0.267	0.059
2.02	0.879	0.892	1.165	3.49	0.266	0.266	0.055
2.05	0.881	0.892	1.125	3.52	0.264	0.264	0.051
2.08	0.882	0.891	1.088	3.55	0.263	0.263	0.047
2.11	0.884	0.891	1.041	3.58	0.262	0.262	0.043
2.14	0.885	0.891	0.986	3.61	0.261	0.261	0.038
2.17	0.886	0.89	0.934	3.64	0.259	0.259	0.034
2.2	0.886	0.89	0.893	3.67	0.256	0.256	0.029
2.23	0.887	0.89	0.869	3.7	0.254	0.254	0.025
2.26	0.887	0.889	0.846	3.73	0.252	0.252	0.021
2.29	0.887	0.889	0.824	3.76	0.249	0.249	0.018
2.32	0.887	0.889	0.794	3.79	0.247	0.247	0.014
2.35	0.887	0.888	0.748	3.82	0.246	0.246	0.01
2.38	0.887	0.888	0.73	3.85	0.244	0.244	0.007
2.41	0.886	0.887	0.712	3.88	0.242	0.242	0.004
2.44	0.884	0.884	0.694				

Tirupati, 1992.

## References

- [1] J.-P. Charles, G. Bordure, A. Khoury and P. Mialhe, "Consistency of the double exponential model with physical mechanisms of conduction for a solar cell under illumination" *J. Phys. D: Appl. Phys.*, 18 (1985) 2261.
- [2] S. R. Kodigala, Ph.D. Thesis, Sri Venkateswara University, Tirupati, 1992.
- [3] M. R. AlRashidi, M. F. AlHajri, K. M. El-Naggar, A. K. Al-Othman, "A new estimation approach for determining the I-V characteristics of solar cells", *Solar Energy* 85 (2011) 1543–1550 doi: 10.1016/j.solener.2011.04.013.
- [4] X. Ma, S. Bader, B. Oelmann, "On the Performance of the Two-Diode Model for Photovoltaic Cells Under Indoor Artificial Lighting", *IEEE Access* 9 (2020): 1350-1361.

- [5] Safae AAZOU & El Mahdi ASSAID, "Modelling Real Photovoltaic Solar Cell Using Maple", in: International Conference on Microelectronics - ICM, 2009 - ieexplore.ieee.org DOI: 10.1109/ICM.2009.5418600.
- [6] E. Assaid and M. El Aydi, "Exact Analytical Solutions of Diodes Bridge, Maple application center", January 2007. Available online at the electronic address: [http://www.maplesoft.com/applications/app\\_center\\_view.aspx?AID=2039](http://www.maplesoft.com/applications/app_center_view.aspx?AID=2039).
- [7] E. Assaid, E. Feddi and M. El Aydi, "Exact Analytical Expressions of Graëtz Bridge Currents and Voltages Using LambertW Function", The 14th IEEE International Conference on Electronics, Circuits and Systems, Marrakech, Morocco, december 11-14, 2007.
- [8] A. Orioli, A. D. Gangi, "A procedure to calculate the five-parameter model of crystalline silicon photovoltaic modules on the basis of the tabular performance data", Appl Energy 2013; 102: 1160–77.
- [9] W. Xiao, M. G. J. Lind, W. G. Dunford, A., Capel, "Real-time identification of optimal operating points in photovoltaic power systems", IEEE Transactions on Industrial Electronics 53 (4), 1017–1026, 2006.
- [10] Alireza Askarzadeh, Alireza Rezazadeh, "Artificial bee swarm optimization algorithm for parameters identification of solar cell models", Applied Energy 102 (2013) 943–949.
- [11] K Ishaque, Z Salam, S Mekhilef, A Shamsudin, "Parameter extraction of solar photovoltaic modules using penalty-based differential evolution", Appl Energy 2012; 99: 297–308.
- [12] L Sandrolini, M Artioli, U Reggiani, "Numerical method for the extraction of photovoltaic module double-diode model parameters through cluster analysis". Appl Energy 2010; 87: 442–51.
- [13] B Amrouche, A Guessoum, M Belhamel, "A simple behavioural model for solar module electric characteristics based on the first order system step response for MPPT study and comparison", Appl Energy 2012; 91: 395–404.
- [14] Jinlei Ding, Rakesh Radhakrishnan, "A newmethod to determine the optimum load of a real solar cell using the Lambert W-function", Solar Energy Materials & Solar Cells 92 (2008) 1566–1569.
- [15] R. M. Corless, G. H. Gonnet, DE. G. Hare, D. J. Jeffrey, D. E. Knuth, "On the Lambert W-Function", Adv. Comput. Math, 5 (1996) 329.
- [16] Adelmo Ortiz-Conde, Francisco J. Garcí'a Sa'nchez, Juan Muci, "New method to extract the model parameters of solar cells from the explicit analytic solutions of their illuminated I–V characteristics", Solar Energy Materials and Solar Cells 90 (3), 352–361, 2006.
- [17] DSH Chan, JCH Phang, Analytical methods for the extraction of solar-cell single-and double-diode model parameters from I–V characteristics. IEEE Transactions on Electron Devices 34 (2), 286–293. 1987.
- [18] DSH Chan, JR Phillips, JCH Phang Chan, "A comparative study of extraction methods for solar cell model parameters", Solid-State Electronics 29 (3), 329–337, 1986.
- [19] A Jain, A Kapoor, "Exact analytical solutions of the parameters of real solar cells using Lambert W-function", Solar Energy Materials and Solar Cells 81 (2), 269–277, 2004.
- [20] H Saleem, S Karmalkar, "An analytical method to extract the physical parameters of a solar cell from four points on the illuminated J–V Curve", IEEE Electron Device Letters 30 (4), 349–352, 2009.
- [21] Joseph A Jervase, Hadj Bourdoucen and Ali Al-Lawati, "Solar cell parameter extraction using genetic algorithms", Measurement Science and Technology 12 (11), 1922–1925, 2001.
- [22] M Ye, X Wang, Y Xu, "Parameter extraction of solar cells using particle swarm optimization", Journal of Applied Physics 105 (9), 094502–094508, 2009.
- [23] T. Easwarakhanthan, J. Bottin, I. Bouhouch, C. Boutrit., "Nonlinear minimization algorithm for determining the solar cell parameters with microcomputers", Sol Energy 1986; 4: 1–12.
- [24] M. Zagrouba, A. Sellami, M. Bouaïcha, M. Ksouri, "Identification of PV solar cells and modules parameters using the genetic algorithms: Application to maximum power extraction", Solar Energy 84 (5) (2010) 860 – 866.
- [25] H. Wei, J. Cong, X. Lingyun, S. Deyun, "Extracting solar cell model parameters based on chaos particle swarm algorithm", In: International conference on electric information and control engineering (ICEICE); 2011. p. 398–402.
- [26] K. M. El-Naggar, M. R. AlRashidi, M. F. AlHajri, A. K. Al-Othman, "Simulated annealing algorithm for photovoltaic parameters identification", Sol Energy 2012; 86: 266–74.
- [27] C. Dai, W. Chen, Y. Zhu, "Seeker optimization algorithm for digital IIR filter design", IEEE Trans Ind Electron 2010; 57: 1710–8.
- [28] T. Enzenhofer, T. Unold, R. Scheer, H.-W. Schock, 20th European Photovoltaic Solar Energy Conference, Barcelona, (2005), p. 1751.
- [29] S. Taunier, J. S. Kurdi, P. P. Grand, A. Chomont, O. Ramdani, L. Parissi, P. Panheleux, N. Naghavi, C. Hubert, M. B. Farah, J. P. Fauvarque, J. Connolly, O. Roussel, P. Mogensen, E. Mahe, J. F. Guillemoles, D. Lincot, O. Kerrec, "Cu(In,Ga)(S,Se)<sub>2</sub> solar cells and modules by electrodeposition" Thin Solid Films 480–481 (2005) 526.
- [30] H. Du, C. H. Champness, I. Shih, "Results on monocrystalline CuInSe<sub>2</sub> solar cells", Thin Solid Films 480–481 (2005) 37.
- [31] M. Kauk, M. Altosaar, J. Raudoja, A. Jagomagi, M. Danilson, T. Varema, "The performance of CuInSe<sub>2</sub> monograin layer solar cells with variable indium content", Thin Solid Films 515 (2007) 5880.
- [32] L. Stolt, J. Hedstrom, J. Kessler, M. Ruckh, K.-O. Velthaus, H.-W. Schock, "ZnO/CdS/CuInSe<sub>2</sub> thin-film solar cells with improved performance", Appl. Phys. Lett. 62 (1993) 597.
- [33] J. A. M. AbuShama, S. Johnston, T. Moriarty, G. Teeter, K. Ramanathan, R. Noufi, " Properties of ZnO/CdS/ CuInSe<sub>2</sub> solar cells with improved performance", Progress in Photovoltaics: Research and Applications 12 (2004) 39.
- [34] J. Hedstrom, H. Ohlsen, M. Bodegard, A. Kylner, L. Stolt, D. Hariskos, M. Ruck, H. W. Schock, Proceedings of 23rd IEEE Photovoltaic Specialists Conference, (1993), p. 364.
- [35] S. H. Wei, S. B. Zhang, and A. Zunger, "Effects of Ga Addition to CuInSe<sub>2</sub> on its Electronic, Structural, and Defect Properties", Applied Physics Letters 72 (1998) 3199-3201. <https://doi.org/10.1063/1.121548>.

- [36] C. H. Huang, "Effects of Ga Content on Cu(In,Ga)Se<sub>2</sub> Solar Cells Studied by Numerical Modelling", *Journal of Physics and Chemistry of Solids* 69 (2008) 330-334. <https://doi.org/10.1016/j.jpcs.2007.07.093>.
- [37] M. Gloeckler, and J. R. Sites, "Band-gap grading in Cu (In, Ga)Se<sub>2</sub> solar cells", *Journal of Physics and Chemistry of Solids* 66 (2005) 1891-1894. <https://doi.org/10.1016/j.jpcs.2005.09.087>.
- [38] Abdelhakim Mahdjoub and Lazhar Hadjeris, "Reflection loss minimization for a ZnO/CdS/CuInSe<sub>2</sub> photovoltaic cell" *Semiconductor Physics, Quantum Electronics & Optoelectronics*, 2013. V. 16, N 4. P. 379-381.
- [39] T. M. Razykov, C. S. Ferekides, D. Morel, E. Stefanakos, H. S. Ullal, H. M. Upadhyaya, "Solar energy, Solar photovoltaic electricity: Current status and future prospects", *Solar Energy*, 85 (8), p. 1580-1608 (2011).
- [40] I. Repins, M. A. Contreras, B. Egaas, C. DeHart, J. Scharf, C. L. Perkins, B. To, R. Noufi, "19.9%-efficient ZnO/CdS/CuInGaSe<sub>2</sub> solar cell with 81.2% fill factor", *Progr. Photovolt.: Res. Appl.* 16 (3), p. 235-239 (2008).
- [41] A. Gerthoffer, F. Roux, F. Emieux, P. Faucherand, H. Fournier, L. Grenet, S. Perraud, "CIGS solar cells on flexible ultra-thin glass substrates: Characterization and bending test", *Thin Solid Films* 592 (2015): 99-104.
- [42] A. Luque and S. Hegedus (eds), *Handbook of Photovoltaic Science and Engineering*, 1<sup>st</sup> Ed, John Wiley & Sons Ltd, England, 2003. <https://doi.org/10.1002/0470014008>.
- [43] I. Repins, M. A. Contreras, M. Romero, Y. Yan, W. Metzger, J. Li, S. Johnston, B. Egaas, C. DeHart, and J. Schar, "Characterization of 19.9% efficient CIGS absorbers", 33rd IEEE Photovoltaic Specialists Conference, San Diego, California, (2008) 1-6. <https://doi.org/10.1109/PVSC.2008.4922628>.
- [44] P. Jackson, R. Wuerz, D. Hariskos, E. Lotter, W. Witte, and M. Powalla, "Effects of heavy alkali elements in Cu(In, Ga)Se<sub>2</sub> solar cells with efficiencies up to 22.6%", *physica status solidi (RRL)-Rapid Research Letters* 10 (2016) 583-586. <https://doi.org/10.1002/pssr.201600199>.
- [45] G. Hanna, A. Jasenek, U. Rau, and H. W. Schock, "Influence of the Ga-content on the bulk defect densities of Cu(In,Ga)Se<sub>2</sub>", *Thin Solid Films* 387 (2001) 71-73. [https://doi.org/10.1016/S0040-6090\(00\)01710-7](https://doi.org/10.1016/S0040-6090(00)01710-7).
- [46] S. H. Song, K. Nagaich, E. S. Aydil, R. Feist, R. Haley, and S. A. Campbell, "Structure optimization for a high efficiency CIGS solar cell", 35th IEEE Photovoltaic Specialists Conference, IEEE (2010) 002488-002492. <https://doi.org/10.1109/PVSC.2010.5614724>.
- [47] M. A. Green, Y. Hishikawa, E. D. Dunlop, D. H. Levi, J. Hohl-Ebinger, M. Yoshita, and A. W. Ho-Baillie, "Solar cell efficiency tables (Version 53)", *Progress in Photovoltaics: Research and Applications* 27 (2019) 3-12. <https://doi.org/10.1002/pip.3102>.
- [48] T. Kato, "Cu(In,Ga)(Se,S)<sub>2</sub> solar cell research in Solar Frontier", *Progress and current status*, *Japanese Journal of Applied Physics* 56 (2017) 04CA02. <https://doi.org/10.7567/JJAP.56.04CA02>.
- [49] H. S. Ullal, K. Zewelbel, and B. Von Roedern, "Current status of polycrystalline thin-film PV technologies", *Conference Record of the Twenty Sixth IEEE Photovoltaic Specialists Conference - 1997, IEEE (1997) 301-305*. <https://doi.org/10.1109/PVSC.1997.654089>.
- [50] S. Ishizuka, A. Yamada, P. Fons, and S. Niki, "Flexible Cu(In,Ga)Se<sub>2</sub> solar cells fabricated using alkali-silicate glass thin layers as an alkali source material", *Journal of Renewable Sustainable Energy* 1 (2009) 013102. <https://doi.org/10.1063/1.3005376>.
- [51] A. Chirilă, S. Buecheler, F. Pianezzi, F. Bloesch, C. Gretener, A. R. Uhl, C. Fella, L. Kranz, J. Perrenoud, S. Seyrling, S. Verma, S. Nishiwaki, Y. E. Romanyuk, G. Bilger, and A. N. Tiwari, "Highly efficient Cu(In, Ga)Se<sub>2</sub> solar cells grown on flexible polymer films", *Nature Materials* 10 (2011) 857-861. <https://doi.org/10.1038/NMAT3122>.
- [52] M. Yamaguchi, "Radiation resistance of compound semiconductor solar cells", *Journal of applied physics* 78 (1995) 1476 - 1480. <https://doi.org/10.1063/1.360236>.
- [53] L. L. Kazmerski, M. Hallerdt, P. J. Ireland, R. A. Mickelsen, and W. S. Chen, "Optical properties and grain boundary effects in CuInSe<sub>2</sub>", *Journal of Vacuum Science & Technology A: Vacuum, Surfaces, and Films* 1 (1983) 395-398. <https://doi.org/10.1116/1.571928>.
- [54] S. M. Sze, "Physics of Semiconductor Devices", Wiley (1981), 51.
- [55] Henry Mathieu, Cours, "Physique des Semiconducteurs et des Composants Électroniques", 2001, 5<sup>e</sup> édition, DUNOD, p. 124; 137.
- [56] El Hadji Mamadou Keita, Abdoul Aziz Correa, Issa Faye, Chamsdine Sow, Cheikh Sene, Babacar Mbow. Short-Circuit Photocurrent Density Determination of Chalcopyrite Solar Cells and Study of Basic Parameters Under AM0, AM1, AM1.5 Spectra. *Science Journal of Energy Engineering*. Vol. 9, No. 4, 2021, pp. 79-89. doi: 10.11648/j.sjee.20210904.15.
- [57] El Hadji Mamadou Keita, Fallou Mbaye, Bachirou Ndiaye, Chamsdine Sow, Cheikh Sene, Babacar Mbow. Optimizing Structures Based on Chalcopyrite Materials for Photovoltaic Applications. *American Journal of Energy Engineering*. Vol. 10, No. 3, 2022, pp. 53-67. doi: 10.11648/j.ajee.20221003.11.
- [58] Alain Ricaud, "Photopiles Solaires", *De la physique de la conversion photovoltaïque aux filières, matériaux et procédés*. 1997, 1<sup>e</sup> édition, Presses polytechniques et universitaires romandes, p. 40.
- [59] E. M. Keita, B. Mbow, C. Sene, "Perovskites and other framework structure crystalline materials", chap No 22: Framework structure materials in photovoltaics based on perovskites 3D", *OAJ Materials and Devices*, vol 5 (2), (Coll. Acad. 2021), p. 637-708. DOI: 10.23647/ca.md20201511.
- [60] Babacar MBOW, Doctoral Thesis, "Etude des Réponses Spectrales dans le proche Infra-Rouge des Composés Mixtes III-V, Ternaires et Quaternaires, à Base de GaSb et de leurs Dérivés", Université Montpellier II (1992) (p. 45-46; 52-55).
- [61] Michelle Schatzman, Cours et Exercices, *Analyse Numérique, "Une Approche Mathématique"*, 2001, 2<sup>e</sup> édition, DUNOD, p. 211.
- [62] P. J. Dale, A. P. Samantilleke, G. Zoppi, I. Forbes, L. M. Peter, "Characterization of CuInSe<sub>2</sub> material and devices: comparison of thermal and electrochemically prepared absorber layers", *J. Phys. D: Appl. Phys.* 41 (2008) 085105.

- [63] R. A. Mickelsen, W. S. Chen, "High photocurrent polycrystalline thin-film CdS/CuInSe<sub>2</sub> solar cells", Appl. Phys. Lett. 36 (1980) 371.
- [64] R. Scheer, T. Walter, H. W. Schock, M. L. Fearheiley, H. J. Lewerenz, "CuInS<sub>2</sub> based thin film solar cell with 10.2% efficiency", Appl. Phys. Lett. 63 (1993) 3294.
- [65] Subba Ramaiah Kodigala, "Cu(In<sub>1-x</sub>Ga<sub>x</sub>)Se<sub>2</sub> based thin solar cells", 2010, Volume 35, Academic Press, ELSEVIER. Inc.
- [66] M. A. Green, "Tracking solar cell conversion efficiency", Nat Rev Phys 2, 172–173 (2020). <https://doi.org/10.1038/s42254-020-0163-y>.